Research Article

Direct Visualization of Deforming Atomic Wavefunction in Ultraintense High-Frequency Laser Pulses

Jintai Liang [ID],[1] Yueming Zhou [ID],[1] Yijie Liao,[1] Wei-Chao Jiang,[2] Min Li,[1] and Peixiang Lu[1,3]

[1]*School of Physics and Wuhan National Laboratory for Optoelectronics, Huazhong University of Science and Technology, Wuhan 430074, China*
[2]*College of Physics and Optoelectronic Engineering, Shenzhen University, Shenzhen 518060, China*
[3]*Optics Valley Laboratory, Hubei 430074, China*

Correspondence should be addressed to Yueming Zhou; zhouymhust@hust.edu.cn

Interaction of intense laser fields with atoms distorts the bound-state electron cloud. Tracing the temporal response of the electron cloud to the laser field is of fundamental importance for understanding the ultrafast dynamics of various nonlinear phenomena of matter, but it is particularly challenging. Here, we show that the ultrafast response of the atomic electron cloud to the intense high-frequency laser pulses can be probed with the attosecond time-resolved photoelectron holography. In this method, an infrared laser pulse is employed to trigger tunneling ionization of the deforming atom. The shape of the deforming electron cloud is encoded in the hologram of the photoelectron momentum distribution. As a demonstration, by solving the time-dependent Schrödinger equation, we show that the adiabatic deforming of the bound-state electron cloud, as well as the nonadiabatic transition among the distorted states, is successfully tracked with attosecond resolution. Our work films the formation process of the metastable Kramers-Henneberger states in the intense high-frequency laser pulses. This establishes a novel approach for time-resolved imaging of the ultrafast bound-state electron processes in intense laser fields.

1. Introduction

Laser-induced distortion of the electron cloud of atoms and molecules is the intrinsic reason for various nonlinear phenomena of matter [1, 2]. Probing the laser-induced dynamics of the bound electron is of essential importance for understanding the temporal properties of nonlinear processes of matter. With the advanced attosecond techniques [3], various laser-induced electron dynamics, such as the valence electron motion [4], the subcycle AC-stark shift [5], the impulsive response of the bound electron [6], the ultrafast charge migration [7], etc., have been probed with attosecond accuracy. Here, we reveal another interesting ultrafast bound-state electron process of atoms induced by the ultraintense high-frequency laser fields. Previous theoretical studies have shown that when an atom is exposed to an ultraintense high-frequency laser field, the electronic wavefunction is stretched and separated into two parts [8]. The distortion of the wavefunction forms the so-called metastable

Kramers-Henneberger (KH) states [9–11], leading to the stabilization against ionization in ultraintense high-frequency laser fields [12], which is one of the most intriguing phenomena in laser-matter interaction. The KH states also play an important role in accelerating neutral atoms [13] and amplifying air lasing [14, 15]. Although the atomic stabilization and the KH states have attracted extensive theoretical studies thirty years ago [16–22], direct observation of this distorted wavefunction has not been reported. It has been proposed that the electronic structure of the KH states can be deduced from the photoelectron momentum distribution (PEMD) [23]. Recently, it has been shown that the dichotomy of the wavefunction of the KH state would exhibit the double-slit interference pattern in the PEMDs [24], which serves as solid evidence of the existence of the KH states. In these studies, a monochromatic field with constant intensity is considered, wherein the atoms stay in a static KH state. However, in the realistic pulsed fields, the atomic wavefunction evolves from the field-free ground state

to the KH states following the envelope of the laser pulses [22, 25]. Moreover, for a laser pulse with rapid turning on, nonadiabatic transition occurs and then the polychotomy, instead of the dichotomy in the wavefunction, is formed [18, 20]. This turning-on effect plays as the key role in determining the degree of atomic stabilization in the ultraintense laser pulses [18–22, 26, 27]. It is also responsible for the low-energy electron generation in the intense high-frequency laser fields [28–31]. Therefore, observing the evolution of the wavefunction is more appealing. However, this evolution has not yet been observed.

Here, we demonstrate a method based on strong-field photoelectron holography (SFPH) to probe the deforming process of the bound-state electronic wavefunction of hydrogen exposed to the ultraintense XUV laser pulses. The concept of SFPH has been proposed about ten years ago [32]. It originates from the interference of the photoelectrons flying directly to the detector after tunneling ionization and those undergoing a near-forward rescattering [32–34]. The holographic pattern has been experimentally observed in strong-field tunneling ionization in different species of atoms and molecules [35–41] and has attracted extensive theoretical attentions [34, 42–50]. In this work, we employ an infrared (IR) laser pulse to induce tunneling ionization of the atom exposed to the ultraintense XUV laser pulses. The holographic patterns in the PEMDs of tunneling ionization encode dynamic information about the deforming process of the electron cloud induced by the XUV pulses. By numerically solving the time-dependent Schrödinger equation (TDSE), we demonstrate that the adiabatic evolution of the electronic wavefunction with the envelope of the XUV laser pulses can be directly tracked with the SFPH. For the pulse with a more rapid ramp, the nonadiabatic transition among the KH states occurs, which is also unambiguously revealed in the hologram of the PEMDs.

The scheme of our method is illustrated in Figure 1. The distortion of the atom electron cloud by the ultraintense XUV pulses could be intuitively understood in the KH frame [51], in which the time-averaged potential has a double-well structure with the two wells locating at $\pm\alpha_0 = \pm E_0/\omega^2$, where E_0 and ω are the strength and frequency of the field, respectively. For a laser pulse with slowly varying envelope $f(t)$, α_0 should be written as [25, 52] $\alpha_0(t) = f(t)E_0/\omega^2$. In this case, the electron cloud evolves adiabatically following the varying double-well potential. So, it is stretched along the laser polarization direction during the rising edge of the laser pulse and then recovers to the atomic wavefunction when the laser field is falling off (see Supplement, Section 1), as shown in Figure 1(a). To detect the temporal evolution of the electron cloud, an IR pulse with moderate intensity is applied to induce tunneling ionization of the deforming atom. The interference of the direct and the rescattering electron wave packets (EWPs) forms the hologram in the PEMDs. It can be considered as the two-center interference, wherein the centers of the direct and the rescattering EWPs are the tunneling point and the rescattering center, respectively [Figure 1(c)]. The tunneling point depends on the structure of the electron cloud at the instant of tunneling [the red dot in Figure 1(b)]. So, by retrieving the tunneling point from the hologram in the PEMDs, the

structure of the electron cloud and its temporal evolution in the ultraintense XUV pulse is directly tracked.

2. Materials and Methods

To demonstrate our scheme, we solve the three-dimensional TDSE of H in the laboratory frame to obtain the PEMDs (in atomic units) (see Supplement, Section 2),

$$i\frac{\partial \Psi(r,t)}{\partial t} = \left\{ \frac{1}{2}[p + A(t)]^2 - \frac{1}{r} \right\} \Psi(r,t). \tag{1}$$

Here, $A(t) = A_{IR}(t + \tau) + A_{XUV}(t)$ describes the combined vector potential of the XUV and the IR fields. τ is the time delay between the two fields. The IR field $A_{IR}(t + \tau) = A_{IR}(t + \tau)e_z$ is linearly polarized along z-axis and its envelope has the cos-squared shape lasting three optical cycles [Figure 2(a)]. The XUV pulses $A_{XUV}(t) = A_{XUV}(t)[\cos\theta e_z + \sin\theta e_y]$ has the Gaussian-shape envelope and it is polarized with an angle θ with the IR field. Figures 2(b) and 2(c) show the obtained PEMDs in the (p_y, p_z) plane (i.e., p_x=0). The polarization direction of the XUV field are $\theta = 0°$ and $\theta = 45°$, respectively. The frequency of the XUV pulse is $\omega_{XUV} = 3$ a.u. and its intensity is 3×10^{19} W/cm^2 with the full width at half maximum (FWHM) of 10 cycles (~ 0.5 fs). The wavelength and intensity of the IR field are 2400 nm and 1×10^{14} W/cm^2, respectively. (Note that the nondipole effect is significant in the PEMDs for the laser parameters in our calculations. It distorts the PEMDs in the laser propagation direction. However, the PEMD in the plane perpendicular to the laser propagation direction is not affected by the nondipole effect (see Supplement 1, Section 2.3).) The time delay between the two fields is adjusted so that the photoelectron tunneling ionized during the time window where the XUV pulse locates could be driven back to the parent ion to form the hologram in the PEMDs. In our calculations, $\tau = 0.67$ fs. We mention that we have also calculated the PEMD by the IR field alone (see Supplement, Figure S2c). The obtained signal is orders of magnitude lower than that in Figure 2. This is because the ultraintense XUV pulse greatly lowers the ionization potential of H (see Supplement, Figure S1d). Thus, the tunneling ionization rate during the quarter cycle where the IR and the XUV pulses overlap is much higher than that of the IR field alone. The XUV field also induces ionization through single- and few-photon absorption, but the signal in the PEMD is separated from the distribution of tunneling ionization by the IR field (see Supplement, Figure S2). Therefore, the signals in the PEMDs of Figures 2(b) and 2(c) are dominated by IR field induced tunneling ionization during the quarter cycle where the XUV pulse locates [the shading area in Figure 2(a)].

3. Results and Discussion

The horizontal holographic fringes in the PEMDs in Figures 2(b) and 2(c) are clearly seen. For $\theta = 0°$, the fringes are exactly symmetric about $p_y = 0$. While for $\theta = 45°$, the
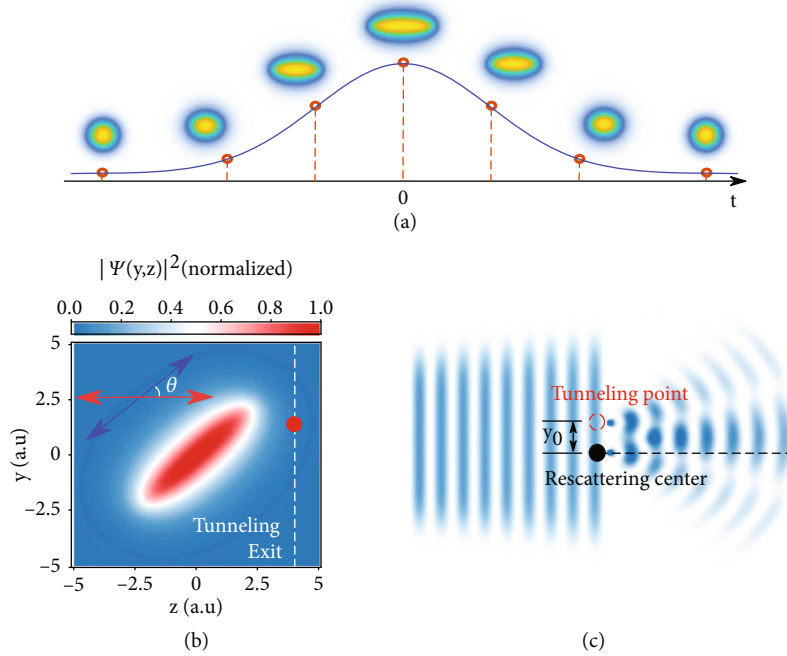
FIGURE 1: (a) Adiabatic evolution of the wavefunction of H in the ultraintense XUV pulse. The solid line denotes the envelope of the intense XUV pulse. (b) The ground-state wavefunction of H with $\alpha_0 = 3.25$ a.u. The blue and red arrows show the polarization direction of the XUV and IR pulses, respectively. Here, the IR field is introduced to probe the deforming wavefunction through tunneling. The red dot denotes the maximum of the cut of the wavefunction at the tunneling exit (the dashed line). It determines the initial transverse displacement y_0 of the tunneling EWP. (c) The principle of our scheme in probing the deforming atom with SFPH. The interference of the direct and the rescattering EWPs in SFPH can be considered as the two-center interference, wherein the centers of the direct and rescattering EWPs locate at y_0 (the tunneling point) and 0 (the rescattering center), respectively. From the hologram in the PEMDs, the tunneling point y_0 can be retrieved and thus the instantaneous shape of the deforming wavefunction is revealed.

interference fringes are distorted. To see this feature more clearly, two cuts from the PEMDs at $p_z = -0.6$ and -1.4 a.u. are shown in Figures 2(d) and 2(e). Obviously, the interference minima (maxima) for $\theta = 45°$ are shifted with respect to the result at $\theta = 0°$. In the following, we will show that the evolution of the deforming wavefunction is encoded in this interference fringes shift.

The holographic fringes are determined by the phase difference between the direct and near-forward rescattering EWPs. With the adiabatic theory [53], the phase difference can be written as [34] (see Supplement, Section 3)

$$\Delta\varphi\left(p_y ; p_z\right) = \frac{1}{2}p_y^2(t_r - t_i) + \sigma + \left[\phi_i(0 ; t_i) - \phi_i\left(p_y ; t_i\right)\right],$$

(2)

where t_i and t_r are the ionization time and rescattering time, respectively. The first term of Equation 2 accounts for the phase difference of the direct and rescattering electrons accumulated during the propagating from tunneling ionization to rescattering [32, 33]. The second term is the phase of the scattering amplitude [34] and for atoms, it is symmetric about the laser polarization direction. In the third term, $\phi_i(p_y ; t_i) = \arg\{\mathscr{A}(p_y ; t_i)\}$ is the phase of the transverse momentum distribution amplitude (TMDA) $\mathscr{A}($

$p_y ; t_i)$ of the tunneling ionization [53, 54]. It accounts for the initial phase difference of the rescattering and the direct electrons. For atoms, $\phi_i(p_y ; t_i)$ is approximately a constant and thus the third term in Equation (2) is absent [34].

When the atom is stretched by the intense XUV field along its polarization direction, there will be a nonzero initial transverse displacement for the tunneling EWP if the angle between the polarization directions of the IR and XUV fields is nonzero, as shown in Figure 1(b). Then, the TMDA has a linear phase distribution. The reason is as follows. The PEMD from tunneling can be approximately considered as the Fourier transform of the tunneling EWP in position space [55, 56]. According to the delay theorem of Fourier transformation, a shift of position of the EWP corresponds to a linear phase in the momentum distribution, $\mathscr{F}[\Psi(y - y_0)] = e^{-iy_0p_y}\mathscr{F}[\Psi(y)]$. Therefore, the phase of the TMDA linearly depends on the initial transverse momentum of tunneling [49, 57, 58]

$$\phi_i\left(p_y ; t_i\right) = -y_0p_y,$$

(3)

where y_0 is the initial transverse displacement of the tunneling EWP. Then, the third term of Equation (2) becomes $\phi_i(0 ; t_i) - \phi_i(p_y ; t_i) = y_0p_y$. So, by extracting this phase from the hologram in the PEMD, we could retrieve the initial transverse
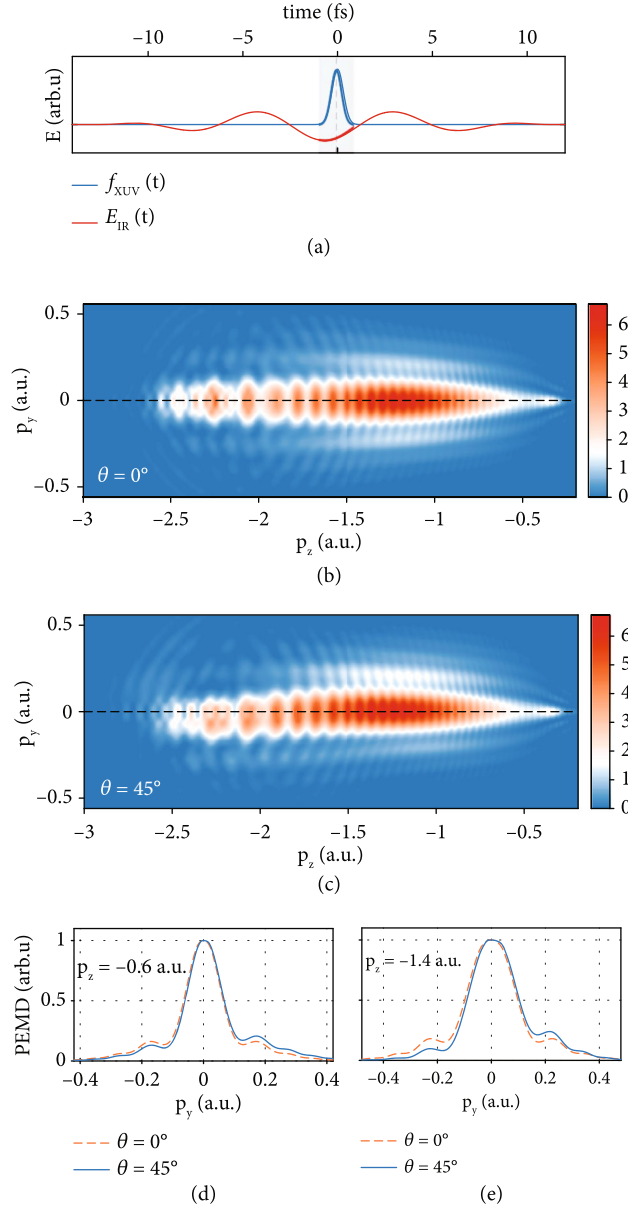
FIGURE 2: (a) The electric field of the IR pulse in our calculations. The blue line represents the envelope of the intense XUV pulse. (b, c) PEMDs from tunneling ionization of H in the XUV-IR pulses, where the angles between polarization directions of the two fields are $\theta = 0°$ and $\theta = 45°$, respectively. (d) The cuts at $p_z = -0.6$ a.u. from (b) and (c). (e) The same as (b) but for the cuts at $p_z = -1.4$ a.u.

displacement y_0 of the tunneling EWP. This displacement is closely related to the structure of the stretched wavefunction. Therefore, by monitoring the initial transverse displacement of the tunneling EWP with SFPH, the structure of the deforming atomic wavefunction can be traced.

The relation between the initial transverse displacement y_0 and the structure of the electronic wavefunction is illustrated in Figures 3(a)–3(c), where we display three examples of the electron density distribution of the stretched atom. In our case, the longitudinal tunneling position is of about 4 ~ 6 a.u. So, we take the cut of the electron density distribution at z~4 a.u. (see Supplement, Figure S5), shown in the right side. In tunneling ionization, the tunneling EWP connects the bound electron wavefunction smoothly, and thus the

transverse displacement of the tunneling EWP equals the position y_m of the maximum of the electron density distribution in the cut around the longitudinal tunneling exit, $y_0 = y_m$. As the atomic wavefunction is stretched longer by the XUV field along its polarization direction, the position y_m increases, and the transverse displacement y_0 increases accordingly. Thus, the quantity y_0 directly reveals how long the atomic wavefunction is stretched at the instant of tunneling ionization.

To retrieve the displacement y_0, we extract the phase $\Delta\varphi(p_y; p_z)$ from the hologram of Figure 2(c) (see Supplement, Section 4). In practice, we separately extract the phase for $p_y > 0$ and $p_y < 0$, denoted as $\Delta\varphi_+(p_y; p_z)$ and $\Delta\varphi_-(p_y; p_z)$,
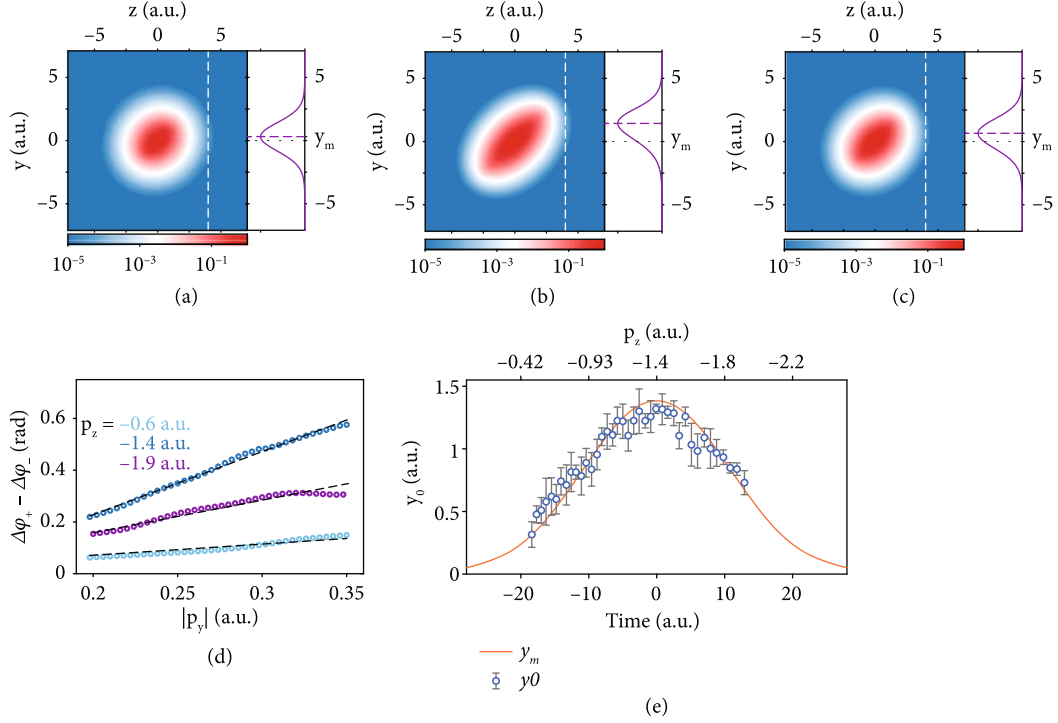
FIGURE 3: (a)–(c) The stretched atomic wavefunctions with $\alpha_0(t) = 1.3, 3.25, 2$ a.u., corresponding to instants of $t = -0.4$, 0 and 0.3 fs of our XUV pulse. The solid curves in the right side show the cuts of the wavefunction at $z = 4.0$ a.u., wherein the dotted lines indicate the maximum y_m of cuts. (d) The phase difference $\Delta\varphi_+(p_y ; p_z) - \Delta\varphi_-(p_y ; p_z)$ extracted from the PEMDs of Figure 2(c) at three cuts $p_z = -0.6, -1.4$, and -1.9 a.u. The dashed lines show the linear fitting. (e) The solid line denotes the maximum y_m of the cut of the stretching wavefunction at the tunneling exit. The circles indicate the transverse displacement y_0 extracted from the PEMD in Figure 2(b). The error bars indicate the 95% confidence interval in fitting. The top and bottom abscissas show the longitudinal momentum and corresponding time, respectively.

respectively (see Supplement, Figure S4). According to Equations (2) and (3), we have

$$\Delta\varphi_+\left(p_y ; p_z\right) - \Delta\varphi_-\left(p_y ; p_z\right) = 2y_0(t_i)\left|p_y\right|. \qquad (4)$$

Equation (4) indicates that the phase difference $\Delta\varphi_+(p_y ; p_z) - \Delta\varphi_-(p_y ; p_z)$ is a linear function of the momentum p_y, with the slope of $2y_0$. Several examples shown in Figure 3(d) indicate that the obtained phase indeed depends linearly with p_y. By fitting this phase with a linear function, the displacement y_0 (half of the obtained slope) is obtained. We repeat this procedure of retrieving y_0 at each p_z in the range $p_z \in [-1.9, -0.4]$ a.u., and transfer the momentum p_z to time through $p_z = -A_{IR}(\tau + t_i)$. The displacement y_0 as a function of time is obtained, displayed in Figure 3(e). It shows that the transverse displacement y_0 increases at the rising edge of the XUV pulse and decreases during the falling edge. This reveals the stretching and restoring of atomic wavefunction with the envelope of the XUV pulse. To check the accuracy of our method, we trace the atomic wavefunction in our calculations, and trace the transverse location y_m for the maximum of the electron density near the longitudinal exit point (see Supplement, Section 5). The result is displayed as the solid curve in Figure 3(e). The agreement is remarkable.

It indicates that the ultrafast deforming of electron wavefunction by the intense XUV pulse is successfully revealed with attosecond resolution by SFPH.

As the duration of the XUV pulse decreases, nonadiabatic transition due to the fast changing envelope becomes significant. Figure 4(a) shows the PEMD from tunneling ionization of the deforming H in a shorter XUV pulse. An intriguing bifurcation structure appears in the PEMDs at (p_y, p_z) = $(-1.65, \pm0.33)$ a.u.. It is more clearly seen in Figure 4(b) where the interference term $\cos\Delta\varphi(p_y ; p_z)$ extracted from the PEMD is shown. This bifurcation structure is due to the nonadiabatic transition in the ultraintense XUV pulses. For the laser parameters in our calculations, nonadiabatic transition results in the electron mainly staying at the ground $1s\sigma_g$ and the excited $2s\sigma_g$ states (see Supplement, Figure S6), i.e., $\Psi(t) = c_1(t)1s\sigma_g + c_2(t)2s\sigma_g e^{i\delta(t)}$, where $\delta(t)$ is the phase difference between these two states. Then, the TMDA for tunneling ionization at time t_i from this superposition is written as $\mathscr{A}(p_y ; t_i) = c_1(t_i)\mathscr{A}_{1s\sigma_g}(p_y) + c_2(t_i)\mathscr{A}_{2s\sigma_g}(p_y)e^{i\delta(t_i)}$, where $\mathscr{A}_{1s\sigma_g}$ and $\mathscr{A}_{2s\sigma_g}$ are, respectively, the TMDA of the $1s\sigma_g$ and $2s\sigma_g$ states, which can be calculated with the method of partial Fourier transformation [56] (see Supplement, Section 6). When $\delta(t_i) = n\pi$ (n is an integer), there is a π phase jump in the TMDA
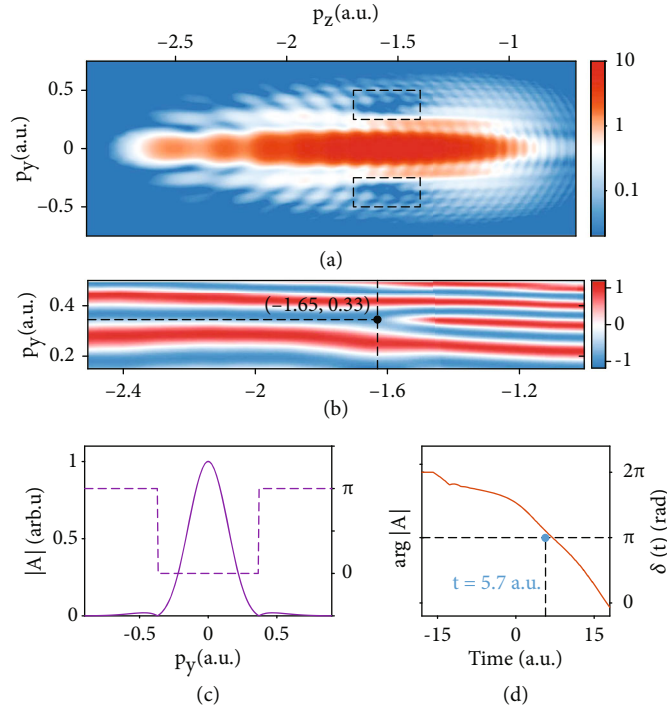
FIGURE 4: (a) PEMD from the tunneling ionization of H atom in the XUV-IR pulse. The FWHM of the XUV pulse is half of that in Figure 2 (5 XUV cycles), and = 90°. The other laser parameters are the same as those in Figure 2. Note that bifurcation structure marked by the dashed box also exit for $\theta = 0°$ and 45°. (b) The extracted interference term of the hologram $\cos\Delta\varphi$ for $p_y > 0$. (c) The modulus (solid line) and phase (dashed line) of the TMDA for the superposition state. (d) The calculated time-dependent phase difference between the $1s\sigma_g$ and $2s\sigma_g$ states (see Supplement, Section 6). The blue dot indicates the π phase difference at the instant of tunneling ionization ($t_i = 5.7$ a.u.) revealed by hologram in (b).

(see Supplement, Figure S7), as shown in Figure 4(c). This phase jump results in the bifurcation structure in the hologram. So, the presence of the bifurcation reveals the nonadiabatic transition in the intense XUV pulse, and the location of the bifurcation indicates the instant when the phase difference between the two occupied states is $n\pi$. In Figure 4(b), the location of $p_z = -1.65$ a.u. corresponds to the ionization time of $t_i = 5.7$ a.u. [obtained through $p_z = -A_{IR}(t_i + \tau)$]. So, the hologram in the PEMD indicates that the phase difference between the $1s\sigma_g$ and $2s\sigma_g$ states at the instant of 5.7 a.u. is $n\pi$. To check the validity of this result, we calculate the phase difference $\delta(t)$ with the time-dependent Floquet Hamiltonian approach [25, 30] (see Supplement, Section 6), as shown in Figure 4(d). The phase difference is indeed close to π at the instant of 5.7 a.u.. So, the nonadiabatic transition and the phase difference between the occupied states are successfully revealed with our method.

4. Conclusion

In conclusion, we filmed the ultrafast evolution of the atomic electron cloud in the ultraintense XUV pulses with SFPH. The distortion of the electron cloud by the XUV fields induces characteristic phase structures in the TMDA of the tunneling EWPs. By measuring the phase structures with SFPH, the adiabatic evolution of the metastable KH states

is accurately tracked, and the nonadiabatic transition among the KH states in the short XUV pulse is also successfully revealed. Our work not only confirms the existence of the KH states but more importantly reveals the ultrafast dynamics of the formation process of the KH states in the ultra-intense XUV pulses. It deepens our understanding of the ultrafast response of bound electron exposed to the intense laser pulses. The dynamic information of bound-state electron is usually delivered to the phase of photoelectrons. So, measuring the photoelectron phase should be an efficient avenue in imaging the attosecond bound electron dynamics [59]. Our work demonstrated a way to track the ultrafast bound-state electron dynamics in atoms by measuring the photoelectron phase with the SFPH. Extension of this method to more complex molecules, and even nanostructures and solids is promising, and it will be a more exciting aspect in the attosecond science.

Data Availability

The data that support the plots within this paper and other findings of this study are available from the corresponding author upon reasonable request.

Conflicts of Interest

The authors declare no conflicts of interest.

Authors' Contributions

Yueming Zhou and Peixiang Lu conceived the study. Jintai Liang performed the calculations and analyzed the data. Yueming Zhou and Jintai Liang wrote the first draft. All authors contributed to interpretation and the final edition of manuscript.

Acknowledgments

Supplementary Materials

Section I in supplemental materials: the KH states of H in ultra-intense XUV laser pulses. Section II in supplemental materials: details of numerically solving TDSE. Section III in supplemental materials: strong-field photoelectron holography in tunneling ionization. Section IV in supplemental materials: procedure of extracting phase from the hologram in the PEMDs. Section V in supplemental materials: details of watching the adiabatic evolution. Section VI in supplemental materials: details of watching the nonadiabatic transition. (*Supplementary Materials*)

References

[1] Y. A. Il'inskii and L. V. Keldysh, *Electromagnetic Response of Material Media*, Springer Science and Business Media, New York, NY, 1994.

[2] E. A. Volkova, A. M. Popov, and O. V. Tikhonova, "Nonlinear polarization response of an atomic gas medium in the field of a high-intensity femtosecond laser pulse," *JETP Letters*, vol. 94, no. 7, pp. 519–524, 2011.

[3] F. Krausz and M. I. Stockman, "Attosecond metrology: from electron capture to future signal processing," *Nature Photonics*, vol. 8, no. 3, pp. 205–213, 2014.

[4] E. Goulielmakis, Z. Loh, A. Wirth et al., "Real-time observation of valence electron motion," *Nature (London)*, vol. 466, no. 7307, pp. 739–743, 2010.

[5] M. Chini, B. Zhao, H. Wang, Y. Cheng, S. Hu, and Z. Chang, "Subcycle ac stark shift of helium excited states probed with isolated attosecond pulses," *Physical Review Letters*, vol. 109, no. 7, article 073601, 2012.

[6] M. T. Hassan, T. T. Luu, A. Moulet et al., "Optical attosecond pulses and tracking the nonlinear response of bound electrons," *Nature*, vol. 530, no. 7588, pp. 66–70, 2016.

[7] P. Kraus, B. Mignolet, D. Baykusheva et al., "Measurement and laser control of attosecond charge migration in ionized iodoacetylene," *Science*, vol. 350, no. 6262, pp. 790–795, 2015.

[8] M. Pont, N. R. Walet, M. Gavrila, and C. W. McCurdy, "Dichotomy of the hydrogen atom in superintense high-frequency laser fields," *Physical Review Letters*, vol. 61, no. 8, pp. 939–942, 1988.

[9] M. Gavrila, "Atomic stabilization in superintense laser fields," *Journal of Physics B: Atomic, Molecular and Optical Physics*, vol. 35, no. 18, pp. R147–R193, 2002.

[10] A. M. Popov, O. V. Tikhonova, and E. A. Volkova, "Strong-field atomic stabilization: numerical simulation and analytical modelling," *Journal of Physics B: Atomic, Molecular and Optical Physics*, vol. 36, no. 10, pp. R125–R165, 2003.

[11] Q. Wei, P. Wang, S. Kais, and D. Herschbach, "Pursuit of the Kramers-Henneberger atom," *Chemical Physics Letters*, vol. 683, pp. 240–246, 2017.

[12] M. Pont and M. Gavrila, "Stabilization of atomic hydrogen in superintense high-frequency laser fields of circular polarization," *Physical Review Letters*, vol. 65, no. 19, pp. 2362–2365, 1990.

[13] U. Eichmann, T. Nubbemeyer, H. Rottke, and W. Sandner, "Acceleration of neutral atoms in strong short-pulse laser fields," *Nature (London)*, vol. 461, no. 7268, pp. 1261–1264, 2009.

[14] M. Richter, S. Patchkovskii, F. Morales, O. Smirnova, and M. Ivanov, "The role of the Kramers-Henneberger atom in the higher-order Kerr effect," *New Journal of Physics*, vol. 15, no. 8, article 083012, 2013.

[15] M. Matthews, F. Morales, A. Patas et al., "Amplification of intense light fields by nearly free electrons," *Nature Physics*, vol. 14, no. 7, pp. 695–700, 2018.

[16] Q. Su, J. H. Eberly, and J. Javanainen, "Dynamics of atomic ionization suppression and electron localization in an intense high-frequency radiation field," *Physical Review Letters*, vol. 64, no. 8, pp. 862–865, 1990.

[17] J. Grochmalicki, M. Lewenstein, and K. Rzyzewski, "Stabilization of atoms in superintense laser fields: is it real," *Physical Review Letters*, vol. 66, no. 8, pp. 1038–1041, 1991.

[18] K. C. Kulander, K. J. Schafer, and J. L. Krause, "Dynamic stabilization of hydrogen in an intense high-frequency pulsed laser field," *Physical Review Letters*, vol. 66, no. 20, pp. 2601–2604, 1991.

[19] K. Burnett, P. L. Knight, B. R. M. Piraux, and V. C. Reed, "Supression of ionization in strong laser fields," *Physical Review Letters*, vol. 66, no. 3, pp. 301–304, 1991.

[20] V. C. Reed, P. L. Knight, and K. Burnett, "Suppression of ionization in superintense fields without dichotomy," *Physical Review Letters*, vol. 67, no. 11, pp. 1415–1418, 1991.

[21] J. H. Eberly and K. C. Kulander, "Atomic stabilization by super-intense lasers," *Science*, vol. 262, no. 5137, pp. 1229–1233, 1993.

[22] M. Y. Ryabikin and A. M. Sergeev, "Stabilization window and attosecond pulse train production at atom ionization in superintense laser field," *Optics Express*, vol. 7, no. 12, pp. 417–426, 2000.

[23] F. Morales, M. Richter, S. Patchkovskii, and O. Smirnova, "Imaging the Kramers–Henneberger atom," *Proceedings of the National Academy of Sciences*, vol. 108, no. 41, pp. 16906–16911, 2011.

[24] P. He, Z. Zhang, and F. He, "Young's double-slit interference in a hydrogen atom," *Physical Review Letters*, vol. 124, no. 16, article 163201, 2020.

[25] K. Toyota, U. Saalmann, and J. M. Rost, "The envelope Hamiltonian for electron interaction with ultrashort pulses," *New Journal of Physics*, vol. 17, no. 7, article 073005, 2015.

[26] Q. Su and J. H. Eberly, "Suppression of ionization and atomic electron localization by short intense laser pulses," *Physical Review A*, vol. 43, no. 5, pp. 2474–2479, 1991.

[27] N. J. Kylstra, R. A. Worthington, A. Patel, P. L. Knight, J. R. Vázquez de Aldana, and L. Roso, "Breakdown of stabilization of atoms interacting with intense, high-frequency laser pulses," *Physical Review Letters*, vol. 85, no. 9, pp. 1835–1838, 2000.

[28] K. Toyota, O. I. Tolstikhin, T. Morishita, and S. Watanabe, "Slow electrons generated by intense high-frequency laser pulses," *Physical Review Letters*, vol. 103, no. 15, article 153003, 2009.

[29] Q. Ning, U. Saalmann, and J. M. Rost, "Electron dynamics driven by light-pulse derivatives," *Physical Review Letters*, vol. 120, no. 3, article 033203, 2018.

[30] J. Liang, W. Jiang, Y. Liao et al., "Intensity-dependent angular distribution of low-energy electrons generated by intense high-frequency laser pulse," *Optics Express*, vol. 29, no. 11, pp. 16639–16651, 2021.

[31] L. Geng, H. Liang, K. Krajewska, L. Y. Peng, and Q. Gong, "Laser-induced electron Fresnel diffraction by XUV pulses at extreme intensity," *Physical Review A*, vol. 104, no. 2, p. L021102, 2021.

[32] Y. Huismans, A. Rouzée, A. Gijsbertsen et al., "Time-resolved holography with photoelectrons," *Science*, vol. 331, no. 6013, pp. 61–64, 2011.

[33] X. Bian, Y. Huismans, O. Smirnova, K. J. Yuan, M. J. J. Vrakking, and A. D. Bandrauk, "Subcycle interference dynamics of time-resolved photoelectron holography with midinfrared laser pulses," *Physical Review A*, vol. 84, no. 4, article 043420, 2011.

[34] Y. Zhou, O. I. Tolstikhin, and T. Morishita, "Near-forward rescattering photoelectron holography in strong-field ionization: extraction of the phase of the scattering amplitude," *Physical Review Letters*, vol. 116, no. 17, article 173001, 2016.

[35] D. Hickstein, P. Ranitovic, S. Witte et al., "Direct visualization of laser-driven electron multiple scattering and tunneling distance in strong-field ionization," *Physical Review Letters*, vol. 109, no. 7, article 073004, 2012.

[36] M. Meckel, A. Staudte, S. Patchkovskii et al., "Signatures of the continuum electron phase in molecular strong-field photoelectron holography," *Nature Physics*, vol. 10, no. 8, pp. 594–600, 2014.

[37] D. G. Arbó, C. Lemell, S. Nagele et al., "Ionization of argon by two-color laser pulses with coherent phase control," *Physical Review A*, vol. 92, no. 2, article 023402, 2015.

[38] S. Walt, N. Ram, M. Atala et al., "Dynamics of valence-shell electrons and nuclei probed by strong-field holography and rescattering," *Nature Communications*, vol. 8, no. 1, article 15651, 2017.

[39] G. Porat, G. Alon, S. Rozen et al., "Attosecond time-resolved photoelectron holography," *Nature Communications*, vol. 9, no. 1, p. 2805, 2018.

[40] M. Li, H. Xie, W. Cao et al., "Photoelectron holographic interferometry to probe the longitudinal momentum offset at the tunnel exit," *Physical Review Letters*, vol. 122, no. 18, article 183202, 2019.

[41] J. Tan, S. Xu, X. Han et al., "Resolving and weighing the quantum orbits in strong-field tunneling ionization," *Advanced Photonics*, vol. 3, article 035001, 2021.

[42] M. Liu, M. Li, C. Wu, Q. Gong, A. Staudte, and Y. Liu, "Phase structure of strong-field tunneling wave packets from molecules," *Physical Review Letters*, vol. 116, no. 16, article 163004, 2016.

[43] W. Yang, H. Zhang, C. Lin et al., "Momentum mapping of continuum-electron wave-packet interference," *Physical Review A*, vol. 94, no. 4, article 043419, 2016.

[44] X. Lai, S. Yu, Y. Huang et al., "Near-threshold photoelectron holography beyond the strong-field approximation," *Physical Review A*, vol. 96, no. 1, article 013414, 2017.

[45] Q. Xia, J. Tao, J. Cai, L. Fu, and J. Liu, "Quantum interference of glory rescattering in strong-field atomic ionization," *Physical Review Letters*, vol. 121, no. 14, article 143201, 2018.

[46] B. Willenberg, J. Maurer, U. Keller et al., "Holographic interferences in strong-field ionization beyond the dipole approximation: the influence of the peak and focal-volume-averaged laser intensities," *Physical Review A*, vol. 100, article 033417, 2019.

[47] S. Brennecke, N. Eicke, and M. Lein, "Gouy's phase anomaly in electron waves produced by strong-field ionization," *Physical Review Letters*, vol. 124, no. 15, article 153202, 2020.

[48] N. Werby, A. Natan, R. Forbes, and P. H. Bucksbaum, "Disentangling the subcycle electron momentum spectrum in strong-field ionization," *Physical Review Research*, vol. 3, no. 2, article 023065, 2021.

[49] M. He, Y. Li, Y. Zhou, M. Li, W. Cao, and P. Lu, "Direct visualization of valence electron motion using strong-field photoelectron holography," *Physical Review Letters*, vol. 120, no. 13, article 133204, 2018.

[50] J. Tan, Y. Zhou, M. He et al., "Determination of the ionization time using attosecond photoelectron interferometry," *Physical Review Letters*, vol. 121, no. 25, article 253203, 2018.

[51] H. A. Kramers, "Collected Scientific Papers (North-Holland, Amsterdam, 1956)WC. Henneberger," *Physical Review Letters*, vol. 21, p. 838, 1968.

[52] K. Toyota, O. I. Tolstikhin, T. Morishita, and S. Watanabe, "Siegert-state expansion in the Kramers-Henneberger frame: interference substructure of above-threshold ionization peaks in the stabilization regime," *Physical Review A*, vol. 76, no. 4, article 043418, 2007.

[53] O. I. Tolstikhin and T. Morishita, "Adiabatic theory of ionization by intense laser pulses: finite-range potentials," *Physical Review A*, vol. 86, no. 4, article 043417, 2012.

[54] P. Batishchev, O. I. Tolstikhin, and T. Morishita, "Atomic Siegert states in an electric field: transverse momentum distribution of the ionized electrons," *Physical Review A*, vol. 82, no. 2, article 023416, 2010.

[55] M. Ivanov, M. Spanner, and O. Smirnova, "Anatomy of strong field ionization," *Journal of Modern Optics*, vol. 52, no. 2-3, pp. 165–184, 2005.

[56] R. Murray, W. K. Liu, and M. Y. Ivanov, "Partial Fourier-transform approach to tunnel ionization: atomic systems," *Physical Review A*, vol. 81, no. 2, article 023413, 2010.

[57] S. Eckart, "Holographic angular streaking of electrons and the Wigner time delay," *Phys. Rev. Research*, vol. 2, no. 3, article 033248, 2020.

[58] D. Trabert, S. Brennecke, K. Fehre et al., "Angular dependence of the Wigner time delay upon tunnel ionization of H_2," *Nature Communications*, vol. 12, p. 1697, 2021.

[59] C. Faria and A. Maxwell, "It is all about phases: ultrafast holographic photoelectron imaging," *Reports on Progress in Physics*, vol. 83, no. 3, article 034401, 2020.